PHILOSOPHICAL TRANSACTIONS A

rsta.royalsocietypublishing.org

Research

Cite this article: Vanderfleet OM, Osorio DA, Cranston ED. 2018 Optimization of cellulose nanocrystal length and surface charge density through phosphoric acid hydrolysis. *Phil. Trans. R. Soc. A* **376**: 20170041.
http://dx.doi.org/10.1098/rsta.2017.0041

Accepted: 23 August 2017

One contribution of 14 to a discussion meeting issue 'New horizons for cellulose nanotechnology'.

Subject Areas:
materials science, nanotechnology, chemical engineering

Keywords:
design of experiments, nanocellulose, acid hydrolysis, atomic force microscopy, phosphate content, thermal properties

Author for correspondence:
Emily D. Cranston
e-mail: ecranst@mcmaster.ca

Electronic supplementary material is available online at http://dx.doi.org/10.6084/m9.figshare.c.3935773.

THE ROYAL SOCIETY PUBLISHING

Optimization of cellulose nanocrystal length and surface charge density through phosphoric acid hydrolysis

Oriana M. Vanderfleet[1], Daniel A. Osorio[2] and Emily D. Cranston[1]

[1]Chemical Engineering Department, McMaster University, 1280 Main Street West, Hamilton, Ontario, Canada L8S 4L8
[2]Materials Science and Engineering Department, McMaster University, 1280 Main Street West, Hamilton, Ontario, Canada L8S 4L8

EDC, 0000-0003-4210-9787

Cellulose nanocrystals (CNCs) are emerging nanomaterials with a large range of potential applications. CNCs are typically produced through acid hydrolysis with sulfuric acid; however, phosphoric acid has the advantage of generating CNCs with higher thermal stability. This paper presents a design of experiments approach to optimize the hydrolysis of CNCs from cotton with phosphoric acid. Hydrolysis time, temperature and acid concentration were varied across nine experiments and a linear least-squares regression analysis was applied to understand the effects of these parameters on CNC properties. In all but one case, rod-shaped nanoparticles with a high degree of crystallinity and thermal stability were produced. A statistical model was generated to predict CNC length, and trends in phosphate content and zeta potential were elucidated. The CNC length could be tuned over a relatively large range (238–475 nm) and the polydispersity could be narrowed most effectively by increasing the hydrolysis temperature and acid concentration. The CNC phosphate content was most affected by hydrolysis temperature and time; however, the charge density and colloidal stability were considered low compared with sulfuric acid hydrolysed CNCs. This study provides insight into weak acid hydrolysis and proposes 'design rules' for CNCs with improved size uniformity and charge density.

This article is part of a discussion meeting issue 'New horizons for cellulose nanotechnology'.

1. Introduction

The extraction of cellulose nanocrystals (CNCs) via hydrolysis of wood and cotton with sulfuric acid was first reported by Nickerson and Habrle in 1947, followed by Rånby in 1949 [1,2]. The hydrolysed particles were found to be highly crystalline and colloidally stable in water [2]. This work inspired Mukherjee & Woods [3], who were the first to image CNCs with transmission electron microscopy. Rod-like particles with lengths of approximately 200 nm and widths of 10–20 nm were observed [3]. The CNC particles tended to form large sheet-like aggregates; however, by increasing the hydrolysis time and temperature, more individualized nanocrystals were obtained [3]. CNCs have since gained popularity both as an academic curiosity and model system to study rod-shaped particles and cellulose interactions, and as an emerging commercial nanomaterial with many potential applications. Importantly, the hydrolysis procedure to produce CNCs from natural cellulose sources is not complex and industry has succeeded in producing ton per day quantities of reproducible and high-quality nanoparticles [4]. Furthermore, the process is relatively green since the starting materials are renewable, the degraded sugar by-products can be fermented for biofuels and the acid can be recycled.

CNCs have many interesting properties; for example, they have a high specific Young's modulus similar to Kevlar and steel, are non-toxic, form lyotropic liquid crystals, and due to their amphiphilic nature and high aspect ratio they are promising reinforcing agents, rheological modifiers and interface stabilizers (e.g. in emulsions, gels and foams) [5]. The colloidal stability of CNCs is another crucial property for most applications and is attributed to the charged surface groups that are grafted onto CNCs during production [5]. Most commonly, CNCs are made by hydrolysis with sulfuric acid, which yields sulfate half-ester groups on the surface, or by strong oxidation which imparts carboxylate groups [6]. Other acids have been used to hydrolyse cellulose, including strong acids such as hydrochloric and hydrobromic acids, as well as weak acids such as phosphoric, citric, oxalic and maleic acids [7–10]. This paper focuses on CNCs produced via phosphoric acid hydrolysis and examines the range of properties attainable using this procedure.

CNCs have potential applications spanning composites, food, cosmetics, packaging, construction, oil and gas, paints, coatings and biomedical devices, to name just a few. While water-based applications and processing methods are the most straightforward for CNCs, there are also many surface modification routes to improve their dispersibility in polymer matrices and increase their compatibility with hydrophobic materials and non-polar solvents [11,12]. For most applications, CNCs with narrow size distributions, tailorable charge content and high yield and crystallinity are required. Although CNCs can be produced from many cellulose sources and under a wide range of hydrolysis conditions [6], the yield and charge content can be very low or the CNCs can be large and aggregated if the conditions are not optimal. For these reasons, past studies have aimed to optimize the sulfuric acid hydrolysis of CNCs [13–20], which is the most widespread hydrolysis procedure and is currently the method of choice for industrial production. These studies have demonstrated that the hydrolysis time, hydrolysis temperature, sulfuric acid concentration and the acid-to-pulp ratio have the most significant effects on CNC properties and end uses.

In general, the optimization and modelling of sulfuric acid hydrolysed CNCs show the same trends and some broad conclusions can be drawn: by increasing the harshness of the hydrolysis (i.e. increasing time, temperature, acid concentration or acid-to-pulp ratio), smaller CNCs with higher sulfate content are typically produced and in higher yield [13–20]. However, if the harshness of the hydrolysis increases beyond a certain point, CNC crystallinity is compromised and the cellulose is degraded into sugars, which can proceed further to form furfurals [18]. This

causes the CNC yield to decrease, while the yield of by-products increases [19]. The optimal hydrolysis conditions for the production of CNCs depend on the desired output parameter, as higher CNC yields have been obtained by lowering the sulfuric acid concentration; however, this resulted in CNCs with lower surface charge density and reduced colloidal stability [19].

Thermal stability of CNCs is another important consideration for many applications, specifically in oil and gas extraction fluids and in the fabrication of nanocomposites which are often processed at high temperatures. The effects of hydrolysis conditions on the thermal stability of sulfuric acid hydrolysed CNCs have been studied and it has been shown that longer hydrolysis times produce CNCs that degrade at lower temperatures [17]. Although improved thermal stability was achieved with very low hydrolysis times, the CNCs produced were larger with lower colloidal stability [17]. Recently, hydrolysis procedures with acids other than sulfuric acid have been used to produce CNCs with increased thermal stability [7,10]. Chen *et al*. [10] used oxalic acid to produce thermally stable CNCs functionalized with carboxyl groups; however, the CNC yield was very low. Work by Camarero-Espinosa *et al*. [7] has demonstrated that CNCs hydrolysed with hydrochloric acid or phosphoric acid have significantly higher thermal degradation temperatures than those hydrolysed with sulfuric acid. Unfortunately, CNCs hydrolysed with hydrochloric acid are uncharged and largely aggregated, do not form colloidal suspensions in water, and as a result are difficult to handle and disperse. Conversely, CNCs hydrolysed with phosphoric acid have anionic phosphate half-ester groups grafted to their surfaces and form stable suspensions, though the colloidal stability of these suspensions does not rival that of CNCs produced with sulfuric acid [7].

The significant improvement in thermal stability of phosphoric acid hydrolysed CNCs is a potential solution for many applications requiring temperature resistance. Furthermore, phosphorylation of (macro)cellulose and cellulose derivatives has been shown to impart flame retardancy [21–24]. On a nanoscale, phosphorylated cellulose nanofibrils have also been demonstrated to possess self-extinguishing properties [25]. We also have interest in CNCs hydrolysed with phosphoric acid because they have potential advantages over their sulfuric acid counterparts as bone scaffolding materials. Other phosphorylated cellulose substrates have demonstrated potential as biomedical materials that promote the formation of hydroxyapatite, which is the inorganic component of bone [26–29]. Thus, not only are CNCs hydrolysed with phosphoric acid stable at high temperatures and potentially flame-retardant, they could ideally be used in bone scaffolding applications to encourage new bone growth.

To facilitate the use of CNCs hydrolysed with phosphoric acid in some of the applications described above, the hydrolysis procedure needs to be optimized and better understood. Although this method has been used in the literature [30,31], the resulting particles are often larger than sulfuric acid hydrolysed CNCs and tend to aggregate due to their low surface charge density [7,32,33]. These shortcomings make the CNCs difficult to work with; post-processing purification such as filtration of CNCs after sonication becomes extremely difficult and results in the loss of material as the aggregates are unable to pass through the normal paper or glass microfibre filters. We hypothesize that the previously demonstrated phosphoric acid hydrolysis protocols are not harsh enough to fully degrade the less-ordered cellulose regions to yield individualized nanoparticles and do not functionalize the nanocrystal surfaces with a sufficient density of phosphate groups. The goal of this project is to optimize the hydrolysis to extract phosphated CNCs that have greater colloidal stability and more uniform size distributions (and thus more predictable performance). A design of experiments (DOE) approach was selected to screen the effects of hydrolysis time, temperature and acid concentration on the morphology, charge content, thermal stability, crystallinity and colloidal stability of CNCs hydrolysed with phosphoric acid.

2. Material and methods

(a) Materials

Phosphoric acid (85 wt%), sodium hydroxide (96 wt%) and sodium chloride (salt) were purchased from Caledon Laboratories Ltd (Georgetown, Canada) and used as received. Dialysis tubing

(14 kDa molecular weight cut-off) was purchased from Sigma-Aldrich. Whatman ashless filter aid (catalogue no.1703-050) and Whatman glass microfibre filter paper was obtained from GE Healthcare Life Sciences Canada. PhosVer 3 Phosphate Reagent Powder Pillows were obtained from Hach Canada. Poly(allylamine hydrochloride) (PAH, Mw 120 000–200 000 g mol^{-1}) was purchased from PolySciences (Warrington, USA) and used without further purification. All water used had a resistivity of 18.2 MΩ·cm and was purified by a Barnstead GenPure Pro water purification system from Thermo Fisher Scientific (Waltham, USA).

(b) Experimental design

A three-factor DOE was chosen to study the effects of hydrolysis time (x_1), temperature (x_2) and phosphoric acid concentration (x_3) on CNC properties. A full factorial of experiments was performed to gain information on the individual effects of the three parameters as well as their two-factor interactions. This full factorial required the extraction of eight batches of CNCs and an additional centre point with conditions (0, 0, 0) was performed as well. The hydrolysis time, temperature and acid concentration had low and high values of 80 min and 120 min, 100°C and 120°C and 70 wt% and 75 wt%, respectively. All three parameters were selected to vary within ranges that would generate a reliable model that could accurately predict CNC properties. The goal of these experiments was to assess which parameters affected the desired outputs most and to determine the direction for future experiments. For this reason, the hydrolysis time, temperature and acid concentration were varied over relatively narrow ranges. Additionally, some constraints further restricted the selected values (like the solubility of cellulose in H_3PO_4). The range of hydrolysis temperatures was initially set to vary from 80 to 120°C; however, acid hydrolysis of cotton at 80°C failed to produce particles with nanoscale dimensions and coagulated/partially digested cellulose was obtained. As discussed below, sample discoloration and burning were observed at 120°C such that higher temperatures could not be used. Furthermore, the range of acid concentrations considered in this paper is narrow because the hydrolysis conditions had to be harsher than those presented by Camarero-Espinosa *et al*. without causing the cellulose to dissolve, which occurs around 80 wt% phosphoric acid [7,34]. For all hydrolyses, CNC length, height, apparent size by dynamic light scattering, phosphate content, thermal stability, crystallinity and zeta potential were measured; however, statistical analysis was only carried out for properties that changed outside of the measurement precision. As such, a linear least-squares regression as a function of the three input parameters was performed for three outputs: CNC length, phosphate content and zeta potential. This statistical analysis was performed in R v. 3.2.3, which is a free and open source statistical computing and graphics program available online (https://cran.r-project.org/).

(c) Phosphoric acid hydrolysis

CNCs were hydrolysed with phosphoric acid roughly following the procedure outlined by Camarero-Espinosa *et al*. [7]. A total of nine hydrolyses were completed with the reaction parameters indicated in table 1 and the naming of samples follows 'hydrolysis time, temperature, acid concentration', i.e. sample 120-120-75 was produced through a 120 min hydrolysis, at 120°C with 75 wt% phosphoric acid. In general, a cotton pulp was first produced by blending 2 g of Whatman ashless filter aid with varying amounts of water, depending on the desired acid concentration. The size of this pulp (with dry density *ca* 0.23 g ml^{-1}) and morphology of its fibres (with diameters *ca* 25 µm) are shown in electronic supplementary material, figure S1. The pulp was placed in a 500 ml round-bottom flask, to which phosphoric acid was added (total volume 361 ml) and the mixture was heated in an oil bath under constant stirring with a magnetic stir bar. Following the hydrolysis, the suspension was cooled in an ice bath and quenched with 600 ml of water. The suspension was evenly divided into six 250 ml Nalgene bottles and centrifuged for 15 min at 3600 r.p.m. in a Sorvall RC-5 superspeed refrigerated centrifuge from Dupont. The resulting supernatant was poured off, an additional 600 ml of water was added to the

Table 1. Properties of CNCs hydrolysed with phosphoric acid with varying hydrolysis time, temperature and acid concentration.

sample name	time, x_1 (min)	temp., x_2 (°C)	acid conc., x_3 (wt%)	zeta potential (mV)	apparent DLS size (nm)	phosphate content (mmol kg^{-1} CNC)	median particle length (nm)	crystallinity index (%)
80-100-70	80	100	70	-10.8 ± 0.6	240 ± 11	15 ± 2	475	96
80-120-70	80	120	70	-11.7 ± 0.5	243 ± 8	31 ± 1	284	97
80-100-75	80	100	75	-9.8 ± 0.7	246 ± 8	8 ± 1	312	96
80-120-75	80	120	75	-17.3 ± 0.8	163 ± 3	13 ± 3	238	96
100-110-72.5	100	110	72.5	-9.0 ± 0.5	215 ± 9	13 ± 1	325	93
120-100-70	120	100	70	-9.8 ± 0.7	250 ± 2	10 ± 1	391	97
120-120-70	120	120	70	-12.4 ± 0.5	200 ± 10	44 ± 2	268	94
120-100-75	120	100	75	-12.4 ± 0.4	179 ± 7	18 ± 11	315	93
120-120-75	120	120	75	-11 ± 1	351 ± 6	17 ± 8	N/A	65

remaining suspension and the centrifugation cycle was repeated. After two centrifugation cycles, the remaining suspension was placed in dialysis. CNCs were dialysed against purified water (suspension : water volume ratio = 20 : 1) changing the water daily until the pH of the suspension no longer changed (*ca* 15 days). Once removed from dialysis, the CNC suspensions were sonicated for 15 min at 60% output with a probe sonicator (Sonifier 450, Branson Ultrasonics) in an ice bath to maintain the temperature below 30°C, and filtered with a glass microfibre filter with 1 µm pore size. CNCs were then converted to the sodium-salt form by adding sodium hydroxide until the samples reached a pH of 7.

(d) Atomic force microscopy

CNCs were imaged by atomic force microscopy (AFM) to study particle morphology. Silica wafers were cleaned with a piranha solution (3 : 1 sulfuric acid to hydrogen peroxide), followed by a rinsing step with water and a drying step with nitrogen. A thin layer of 0.1 wt% PAH was spin-coated (G3P spin-coater, Specialty Coating Systems, Inc.) onto the wafers at 4000 r.p.m. for 30 s to prevent aggregation of the CNCs. Following the deposition of PAH, water was spin coated to rinse the substrate. Lastly, a dilute CNC suspension (0.01 or 0.005 wt%) was spin coated onto the wafers. Images were collected on a MFP-3D AFM (Asylum Research an Oxford Instruments Company, Santa Barbara, USA) in tapping mode. FMR cantilevers, with a force constant of 2.8 ± 0.7 N m^{-1} and a resonance frequency of 75 ± 15 Hz, were purchased from NanoWorld and used to collect images. Post-processing of the images was performed with Asylum Research 13.17 software, in conjunction with Igor Pro 6.37. Images were flattened with the Magic Mask feature and the particle size distributions were obtained using the built-in particle analysis tool in the Asylum Research software. All edge particles were ignored and any particles with areas less than 25 nm^2 were not measured. CNC particle length and particle cross section (from the height profile) were measured on the height images [35]. The particle size distributions shown here and in the electronic supplementary material are all the result of particle counts greater than 100, over multiple AFM images. Owing to the nature of the samples and the presence of large aggregates, the median CNC length was selected rather than the average CNC length to best represent CNC size. Further justification for choosing the median CNC length for statistical modelling is described in the electronic supplementary material, figure S2 (as tested on shorter and more dispersed sulfuric acid hydrolysed CNCs).

(e) Dynamic light scattering

Apparent CNC size in suspension was obtained by dynamic light scattering (DLS) with a Malvern ZetaSizer Nano at 25°C for 0.025 wt% CNC suspensions. The term 'apparent' is used to recognize the limitation of DLS which assumes spherical particles; since CNCs are rod shaped the DLS values can only be used as a relative measure but do provide insight regarding size, size distribution and degree of aggregation of CNCs in suspension [36]. Three particle size estimates were obtained for each sample; each estimate is an average particle size obtained from a distribution of values collected over 10–15 measurements. The sample average with 95% confidence (assuming normal distribution) is reported from three measurements.

(f) Colorimetric determination of phosphate

Colorimetric methods have been used to detect phosphate levels in solution for decades [37–39]. Readily available powder pillows from Hach are commonly used to detect phosphates in water samples with a portable spectrophotometer. This method is comparable to standard procedures outlined in the literature [40]. Dilute CNC suspensions of 0.1 wt% were prepared for phosphate content analysis. The CNC suspension was placed in the Hach DR 2800 portable spectrophotometer and the absorbance of the sample at a wavelength of 880 nm was measured. This absorbance was used as a blank. A PhosVer 3 Ascorbic Acid Powder Pillow from Hach was added to a separate CNC suspension. This sample was vigorously mixed for 30 s, followed by a 2 min wait time for the reaction to proceed to completion. The reactive orthophosphate in the CNC sample reacts with the molybdate from the powder pillows under acidic conditions to form a phosphomolybdic complex, which appears blue in colour. The absorbance of this sample was measured at 880 nm and translated to a phosphate content. The sample average with 95% confidence (assuming normal distribution) is reported from three measurements.

(g) Zeta potential

Zeta potential was used to assess the colloidal stability of the CNCs in suspension and was measured with a ZetaPlus zeta potential analyser from Brookhaven Instruments. All zeta potential measurements were performed on 0.1 wt% CNC suspensions with 5 mM NaCl added. Three measurements were performed on each sample and the electrophoretic mobility was converted to zeta potential following Smoluchowski theory. The sample average with 95% confidence (assuming normal distribution) is reported from three measurements.

(h) X-ray diffraction

X-ray diffraction (XRD) was used to determine the degree of crystallinity for CNCs. Freeze-dried CNCs were compressed into small discs and mounted on a silicon wafer. A Bruker D8 Discover diffractometer with Davinci design was used to collect two-dimensional frames at a detector distance of 14 cm. The X-ray source was a cobalt sealed tube emitting an electron beam with a wavelength of 1.79026 Å with a 35 kV and 45 mA power source. The sample was properly positioned with a vertical D8 θ–θ goniometer, while a 0.5 mm micro slit and a 0.5 mm short collimator were used to adjust the beam. One-dimensional frames were obtained by integrating the two-dimensional frames with Diffrac.eva 4.0 and subtracting frames collected on an empty silicon wafer. Rietveld refinement was used to match theoretical models to the measured diffraction spectra for both the crystalline and amorphous phases [41,42]. The amorphous phase was modelled with a pseudo-Voigt function and a manually inserted fixed peak at 24.1° for all samples. Crystallinity index was obtained by comparing the contribution of the crystalline peaks to the diffraction spectrum of the sample. The measurement error is taken to be *ca* 5%.

(i) Thermogravimetric analysis

Thermogravimetric analysis (TGA) was performed on freeze-dried CNCs with a TA Instruments Q50 thermal analyser. To get reproducible TGA results, a round pellet was formed by placing 3.0 mg of dried CNCs between two plastic stoppers in a 1.0 ml syringe. The CNCs were compressed to form a pellet, which was placed in an argon-filled chamber. The mass of the sample was monitored as the temperature in the analyser was raised to 600°C from room temperature at a rate of 10°C min^{-1} under argon.

3. Results and discussion

Nine phosphoric acid hydrolyses covering the desired parameter space were performed to produce phosphated CNCs with a range of properties. (In the following discussion, samples are named according to the convention 'hydrolysis time, temperature, acid concentration'.) CNCs were fully characterized and the zeta potential, apparent particle size, phosphate content, median particle length and crystallinity index are shown in table 1. While AFM length and apparent size by DLS are both size measurements, we include both because one is a physical size but a two-dimensional projection of a three-dimensional system, and the other provides insight into the dispersion of nanoparticles in suspension. In general, the two size measurements show the same trend with hydrolysis conditions—the CNCs produced are shorter with increasing hydrolysis harshness. AFM median lengths span 238–475 nm and apparent size by DLS ranges from 163 to 250 nm which implies that nanoparticles are being produced and that there is no significant aggregation in suspension.

As expected, almost all hydrolysis conditions produced rod-like nanoparticles, as shown in figure 1, except for the harshest hydrolysis (i.e. 120-120-75). The particles extracted from this hydrolysis can be seen in figure 1*i*; they appear to be aggregates of over-hydrolysed, degraded and re-precipitated cellulose and larger micrometre size clumps were also observed but difficult to image by AFM. We do not consider the 120-120-75 CNCs to be true CNCs based on size, the low degree of crystallinity [4] and the brown colour observed after hydrolysis. At first, harsher acid hydrolysis conditions (increased time, temperature and acid concentration) have resulted in increased CNC crystallinity due to degradation of the amorphous regions into oligosaccharides [18]. Beyond a certain point, however, crystallinity has been shown to decrease due to damage to the crystalline region [17], which has likely occurred with 120-120-75. An attempt was made to introduce a cellulose II phase for the 120-120-75 sample. The peaks observed in the XRD spectra of this sample were very broad and, while some peaks resemble those of a cellulose II phase, this cannot be stated with absolute certainty. The XRD profile can be seen in electronic supplementary material, figure S3. Furthermore, the brown colour of the CNCs hydrolysed at the harshest condition is likely due to the formation of fufural and 5-hydroxymethyl-2-furfural (HMF), which are degradation products from the hydrolysis of CNCs. The reaction pathways leading to the formation of these compounds have been discussed in several papers [18,43] and the presence of HMF has previously been quantified via high pressure liquid chromatography [44–46]. As such, due to the presence of large aggregates and the apparent degradation of crystalline regions, the median length/size distribution and statistical analyses were not performed on 120-120-75. The eight remaining samples were used in the DOE modelling and are considered sufficient to obtain model results with confidence levels that can be calculated and do not span zero.

Zeta potential is a measure of colloidal stability, where absolute values over 20 mV are generally taken as colloidally stable suspensions [36]. The CNCs produced using phosphoric acid do not meet this criterion yet appear well dispersed in water and remain stable over time by eye. Small additions of salt (approx. 10 mM), however, will cause the particles to coagulate and settle which supports the zeta potential values reported. The zeta potential is a function of the phosphate content (i.e. surface charge density, see electronic supplementary material, table S1, for surface charge density approximations calculated from phosphate content and

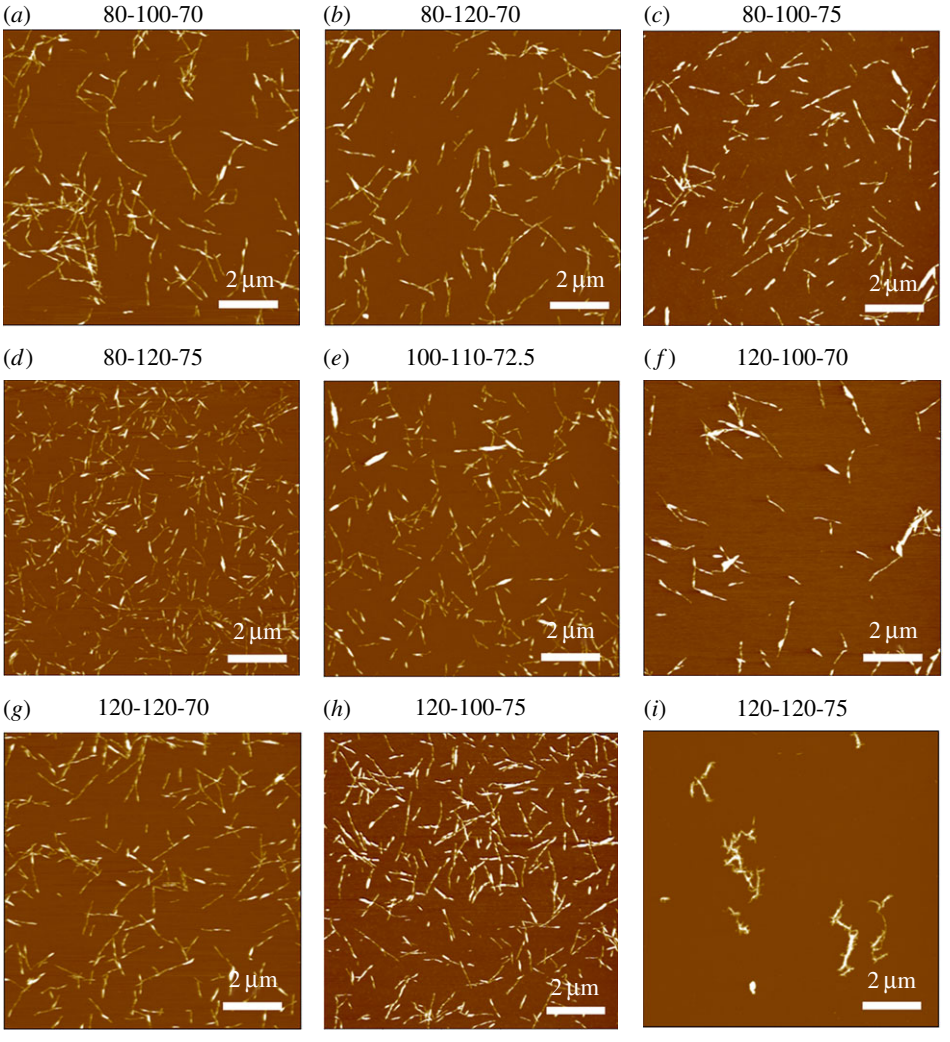

Figure 1. Atomic force microscopy height images of CNCs hydrolysed with phosphoric acid with varying hydrolysis time, temperature and acid concentration (as indicated above each image). Images (*a–i*) roughly follow the order of increasing acid hydrolysis harshness. All scale bars are 2 µm. (Online version in colour.)

AFM particle dimensions) and the particle size and is discussed further below in the modelling section.

The degree of crystallinity for CNCs is important because the mechanical properties, response to electromagnetic fields and chemical resistance are directly related to the organization and packing of polymer chains in the nanoparticles. The degree of crystallinity also relates to the harshness of the hydrolysis where too little or too much hydrolysis of cellulose could lead to significant changes in the crystal structure. All CNCs produced had a high degree of crystallinity, over 93% (except for 120-120-75). From table 1, the crystallinity values are within the assumed measurement error (5%) and were therefore not included in any statistical analysis. We conclude that phosphoric acid hydrolysis yields highly crystalline CNCs, similar to sulfated CNCs, but that within the range of hydrolysis time, temperature and acid concentrations tested we cannot tailor CNC crystallinity to a significant degree.

A primary reason to produce CNCs by phosphoric acid hydrolysis is to obtain more thermally stable CNCs. The TGA curves in figure 2 indicate that all CNCs showed significant increases

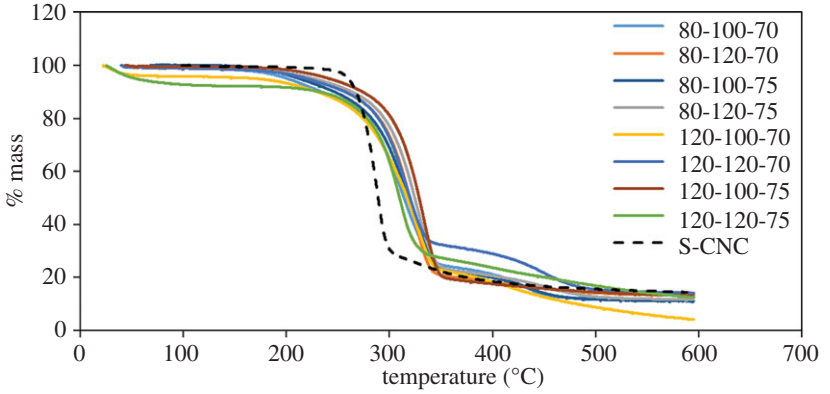

Figure 2. Thermal degradation curves of CNCs hydrolysed with phosphoric acid with varying hydrolysis time, temperature and acid concentration. The dashed black line shows the thermal degradation curve for CNCs hydrolysed with sulfuric acid (S-CNC). (Online version in colour.)

in thermal stability when compared with CNCs hydrolysed with sulfuric acid. Sulfuric acid hydrolysed CNCs in the sodium form are known to be more stable than in the acid form [47] and this is also the case for phosphoric acid hydrolysed CNCs. While the results in figure 2 are for sodium form CNCs, a separate study was performed on CNCs hydrolysed for 90 min at 100°C with 70 wt% phosphoric acid. In the acid form, the CNCs from this sample had a maximum rate of thermal decomposition of 331°C, which is significantly lower than the 392°C observed for the same CNCs in the sodium form. Interestingly, however, very similar thermal degradation patterns were observed for all phosphated CNCs and the thermal stability was not changed in a statistically significant way by changing the hydrolysis conditions. As such, the generation of a model for thermal stability is not included in this paper; future studies will examine thermal degradation mechanisms of CNCs produced with different acids in more detail. The following sections present the DOE models for properties that can be tailored significantly though phosphoric acid hydrolysis and that generate models with high confidence. In order of decreasing model accuracy, CNC length, phosphate content and zeta potential (colloidal stability) are presented below.

(a) Median particle length model

The median particle lengths for each CNC sample were obtained by automated particle detection on AFM images as described above. The *median* particle length was chosen to represent CNC size because it is not heavily affected by aggregates. The particle size distributions were measured for eight samples (all samples except for 120-120-75). CNCs hydrolysed with phosphoric acid have the potential to be tailored over a larger range of lengths compared with CNCs hydrolysed with sulfuric acid, whose lengths do not vary as significantly. Within the range of hydrolysis conditions tested, median length of CNCs hydrolysed with phosphoric acid varied within 238–475 nm. Conversely, research shows that CNCs produced through various sulfuric acid hydrolysis conditions have lengths that either do not change with any statistical significance or change within a smaller range of values (e.g. 130–281 nm) [17,19]. A multiple linear least-squares regression was performed in R and the following model (equation (3.1)) was generated to predict the median particle length (Y) based on hydrolysis time (x_1), hydrolysis temperature (x_2) and phosphoric acid concentration (x_3):

$$Y = 200.65 - 24.51x_1 - 30.18x_2 - 35.81x_3 - 10.00x_1x_2 - 19.38x_2x_3 - 16.99x_1x_3. \quad (3.1)$$

The R^2 (coefficient of determination) for this model is 1 and the p-value is 0.003, suggesting that the null hypothesis should be rejected and this model accurately describes the effects of hydrolysis

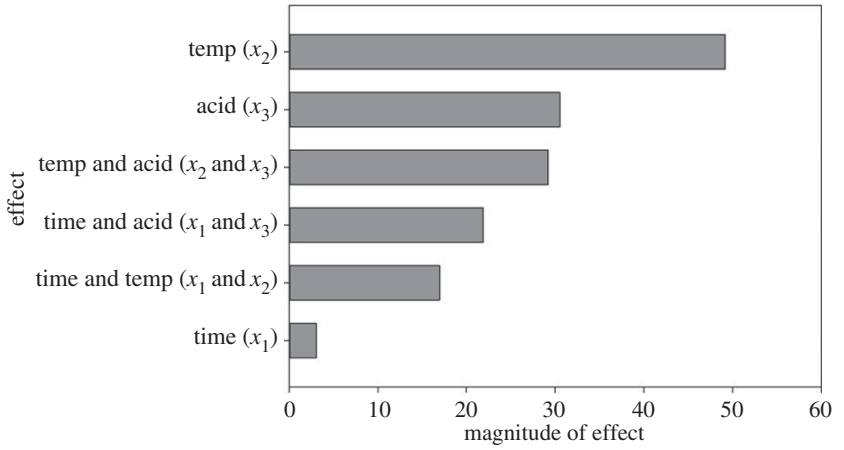

Figure 3. Coefficients for the parameters in a model predicting median CNC length. All coefficients are negative (i.e. an increase in the input parameter results in a decrease of the output property).

parameters on median CNC length. The coefficients for the parameters of this model are shown in figure 3.

The most significant effects on median CNC length were observed by changing the hydrolysis temperature and acid concentration. Previous work by Chen *et al*. [19] has similarly discussed a strong dependence of CNC length on the sulfuric acid concentration used in the hydrolysis. CNCs hydrolysed with phosphoric acid appear to follow the same trend; increasing the acid concentration allows for the extraction of CNCs with a lower median length. Hydrolysis temperature, as well as the interaction between temperature and acid concentration, also play significant roles in determining median CNC length. The strong effect of temperature on CNC length is likely a result of a higher rate constant for the acid hydrolysis of cellulose [48]. Higher rate constants result in faster hydrolysis of glycosidic linkages and lower degree of polymerization of cellulose, which correlates with nanocellulose length [49]. The exact reason for the increase in reaction rate remains unclear; however, both increased diffusion of acid into cellulose fibres and a higher acidity function of phosphoric acid could be responsible [50]. The strong interaction between temperature and acid concentration is evident from both figure 3 and the factor interaction profiles in figure 4. The slopes of the median length versus hydrolysis temperature at low and high acid concentrations have very different magnitudes, indicating a strong interaction between acid concentration and temperature. At a low acid concentration, changes in hydrolysis temperature have greater effects on median CNC length than at a high acid concentration. Similarly, a plot of median length versus acid concentration shows that, at lower temperatures, small changes in acid concentration cause larger decreases in median CNC length. Strong interactions between hydrolysis temperatures and acid concentrations have been observed in other work with sulfated CNCs [18,20]. The degree of hydrolysable cellulose has been shown to increase with increasing reaction harshness; a parameter that was used to designate the combined effect of temperature and acid concentration in a sulfuric acid hydrolysis [18]. The degree of hydrolysable cellulose was defined as the fraction of cellulose that could be de-polymerized at given hydrolysis conditions [18]. A higher degree of hydrolysable cellulose is reflected in shorter CNCs; this was also observed in the CNCs hydrolysed with phosphoric acid. By increasing both the temperature and acid concentration of the hydrolysis, a lower polydispersity of CNCs was observed. Figure 5 shows particle size distributions collected from AFM images of samples 80-100-70 and 80-120-75 which are the least harsh and most harsh hydrolysis conditions with an 80 min hydrolysis time, respectively. (Electronic supplementary material, figure S4, shows particle size distributions for all samples.) By increasing both the temperature and the acid concentration,

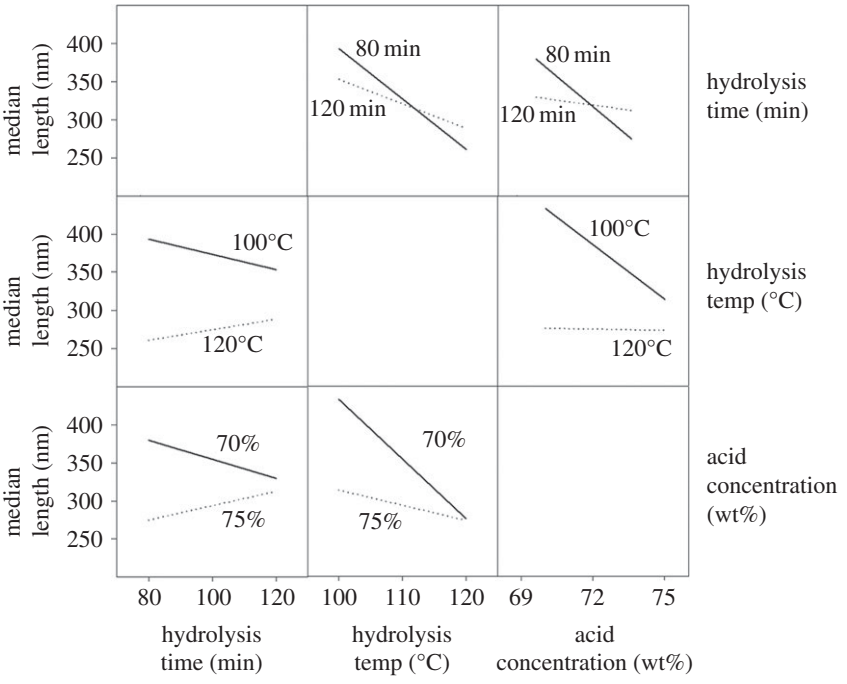

Figure 4. Factor interaction profiles describing the interactions of two hydrolysis parameters and their combined effects on median CNC length.

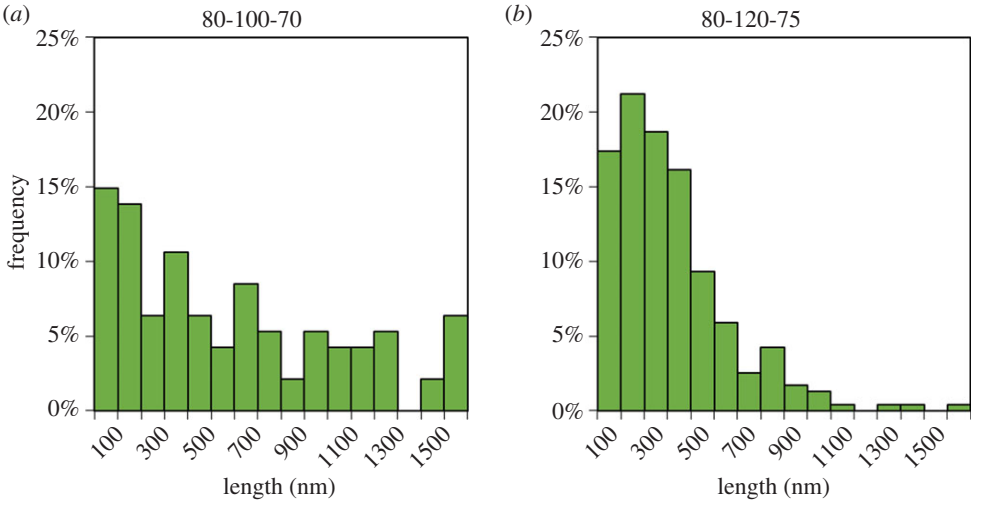

Figure 5. Particle size distributions obtained from AFM image analysis for two CNC batches hydrolysed under different conditions as indicated above each histogram. (Online version in colour.)

the particle size distribution becomes narrower and fewer large CNCs or CNC aggregates are observed. This is also apparent in the AFM images in figure 1.

Conversely, figure 3 shows that hydrolysis time on its own does not significantly affect median CNC length over the range of hydrolysis times tested in this study. This is in line with findings by Kargarzadeh *et al*. [17], where CNCs were hydrolysed with sulfuric acid for 20–120 min and no discerning changes in CNC length were observed. It is possible, however, that a hydrolysis time

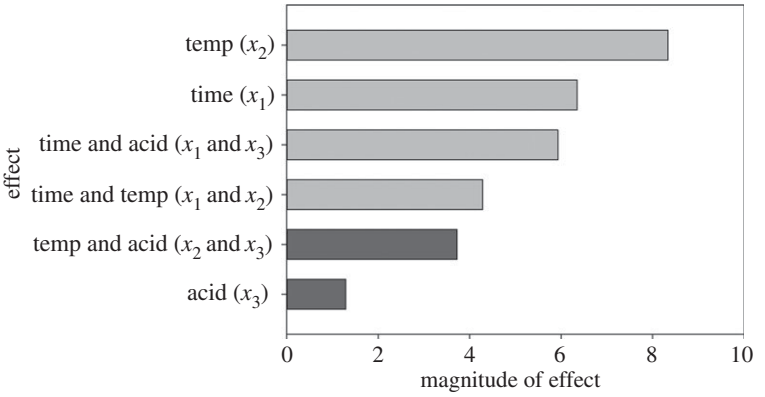

Figure 6. Coefficients for the parameters in a model predicting CNC phosphate content. Light grey bars indicate positive coefficients, while dark grey bars indicate negative coefficients.

significantly lower than 80 min could result in much longer CNCs. The range of hydrolysis times selected for this set of experiments is likely within a plateau region where no further decreases in CNC length can be observed with increasing hydrolysis times.

(b) Phosphate content model

The phosphate content for each sample can be seen in table 1 and the charge density is calculated in the electronic supplementary material, table S1. The lowest and highest observed phosphate contents were 8.2 and 44.5 mmol kg^{-1}, respectively. The surface charge densities span 0.01–0.05 e nm^{-2} which are low compared with sulfated CNCs (80–350 mmol kg^{-1} or *ca* 0.1–1 e nm^{-2}) [4,14,51–53]. A multiple linear least-squares regression was performed and the following model (equation (3.2)) was generated to predict the phosphate content (Y) based on hydrolysis time (x_1), hydrolysis temperature (x_2) and acid concentration (x_3):

$$Y = 23.28 + 6.34x_1 + 8.33x_2 - 1.29x_3 + 4.28x_1x_2 - 3.72x_2x_3 + 5.93x_1x_3. \tag{3.2}$$

The R^2 for this model is 0.8844 and the p-value is 0.59, meaning that there is not enough evidence to reject the null hypothesis. This model cannot fully predict CNC phosphate content; however, it can provide key insights into the main factors affecting charge content on CNCs hydrolysed with phosphoric acid. The coefficients for the parameters of this model are shown in figure 6.

Changes in hydrolysis temperature between 100°C and 120°C have the most significant effects on CNC phosphate content, while the effect of changing acid concentration on its own is minor. Furthermore, the Pareto plot in figure 6 and the sign of the coefficients in the model's equation show that increasing the acid concentration causes phosphate content to slightly decrease, while increasing the hydrolysis time or temperature causes phosphate content to increase. The factor interaction profiles can be found in electronic supplementary material, figure S5. This does not follow previously demonstrated trends for the hydrolysis of CNCs with sulfuric acid. Work by Dong *et al*. [20] concluded that acid concentration had the most significant effect on CNC sulfate content, while hydrolysis temperature had a moderate effect and hydrolysis time had a negligible effect. Chen *et al*. [19] showed that acid concentration has the most drastic effect on CNC sulfate content, though hydrolysis time and temperature were also shown to be important factors. At low acid concentrations, the effects of hydrolysis time were shown to be more significant, as the formation of sulfate half-esters on CNC surfaces occurs relatively slowly. At high acid concentrations, the effects of time are less significant, as CNC sulfate content increases sharply and levels off [19]. The strong effect of acid concentration on the sulfate content for CNCs hydrolysed with sulfuric acid is directly related to the fact that sulfuric acid is a strong acid and is known to catalyse the esterification of cellulose [54].

As mentioned, CNCs hydrolysed with phosphoric acid have roughly one-tenth of the surface charge density of those hydrolysed with sulfuric acid. This is likely related to the fact that phosphoric acid is a weaker acid that is not entirely dissociated in solution and does not catalyse esterification to the same extent as sulfuric acid. Furthermore, to reach the same H^+ concentration in the reaction as is present with approximately 65 wt% sulfuric acid (the most common protocol [55]) would require a phosphoric acid concentration over 15 M (assuming a dissociation constant of *ca* 0.618 [56]); this concentration would dissolve cellulose [34]. (The ratio of ionic species from phosphoric acid dissociation at high concentrations and high temperatures is also somewhat debated [57,58].) We can also infer that our hydrolysis never reaches the same severity in terms of acid concentration, because we do not observe a significant levelling off or decrease in phosphate content, as has been observed with sulfuric acid. Finally, the small changes in phosphate content overall may be a result of insignificant changes in H^+ concentration over the 70–75 wt% range of acid conditions tested. The hydrolysis time and temperature have far more significant effects on phosphate content within this DOE. From these results, we conclude that the most significant effect of the acid strength (strong versus weak acid) is apparent in the ability of the acid to impart surface charge density which unfortunately leads to phosphated CNCs which are not sufficiently charged or colloidally stable for some of the intended applications.

(c) Zeta potential model

As discussed, zeta potential relates to colloidal stability and is a function of the surface charge density and CNC size—the value is calculated from the electrophoretic mobility of the particles in suspension. The zeta potential values are given in table 1 and range from −17.3 mV to −9.0 mV. The zeta potential was measured at pH 7, which is below the second pK_a of phosphoric acid; however, the effect of pH on zeta potential was found to be negligible as shown in electronic supplementary material, figure S6. A multiple linear least-squares regression was performed and the following model (equation (3.3)) was generated to predict the zeta potential (Y) based on hydrolysis time (x_1), hydrolysis temperature (x_2) and acid concentration (x_3):

$$Y = -12.40 - 0.41x_1 - 2.11x_2 - 1.64x_3 - 0.03x_1x_2 - 1.23x_2x_3 - 0.49x_1x_3. \tag{3.3}$$

The R^2 for this model is 0.6969 and the p-value is 0.8426, meaning that there is not enough evidence to reject the null hypothesis. This model cannot fully predict CNC zeta potential. Furthermore, as all zeta potentials are within a small range and they indicate a general lack of colloidal stability for phosphoric acid hydrolysed CNCs, this model will not be discussed extensively. A Pareto plot demonstrating the effects of hydrolysis time, temperature and acid concentration can be seen in the electronic supplementary material, figure S7, and factor interaction profiles are included in the electronic supplementary material, figure S8. Overall, temperature and acid concentration affect the zeta potential the most (which are also the most significant parameters affecting the CNC length) which implies that with the low charge content values obtained here, the size is a dominant factor in predicting how CNCs move in an electric field.

4. Conclusion

This DOE study provided significant insight into the effects of hydrolysis time, temperature and acid concentration on the morphology and surface charge density of CNCs hydrolysed with phosphoric acid. Three main outputs were statistically analysed: CNC length, phosphate content and zeta potential. The intention was to perform a screening study and understand the range of properties attainable through phosphoric acid hydrolysis of cellulose, not to develop a predictive model, as has been done elegantly, for example, in the central composite design study of sulfuric acid hydrolysed CNCs by Dong *et al*. [20]. We also did not investigate the yield from these hydrolyses but observed that in all cases the yield of CNCs produced was greater than 40% and could likely be improved.

The data collected generated models with high confidence for CNC length but could not fully describe the phosphate content and zeta potential results for phosphoric acid hydrolysed CNCs. Nonetheless, general trends were observed to understand which parameters had the greatest effects on these CNC properties. The hydrolysis temperature and phosphoric acid concentration have the greatest effect on median CNC length and on the overall particle size distribution. Increasing both temperature and acid concentration increases the reaction harshness and results in CNCs with a narrower particle size distribution and smaller median length. Hydrolysis time and temperature had the greatest effects on CNC phosphate content, while the effect of acid concentration was negligible. This is because only a small percentage of phosphoric acid is dissociated and small changes in the acid concentration have little effect on the ability to graft phosphate half-esters onto the CNC surfaces. CNCs extracted with phosphoric acid similarly have small zeta potentials which indicates low colloidal stability. Furthermore, the zeta potential values measured did not vary significantly with changing hydrolysis parameters.

Overall, this DOE provided general 'rules' for tailoring CNC size showing that we could control CNC length over a significantly larger range than for sulfated CNCs. This is particularly useful for controlling CNC reinforcement, rheological modification and interface stabilizing abilities. The use of a weak acid gave an expanded range of properties by not degrading the cellulose too quickly under mild hydrolysis conditions. The downfall of using a weak acid is that low phosphate content and low colloidal stability were inevitable. Although the surface charge density and zeta potential could be better modelled by increasing the number of runs and adding second-order variables to the model, the resultant model implied that higher phosphate content can be imparted by using harsher hydrolysis conditions (most importantly, by increasing the hydrolysis temperature). All of the CNCs produced in this work have high crystallinity and thermal stability and we believe this is a good first step towards tailoring phosphated CNC properties to maximize their potential in high temperature applications and biomedical devices.

Data accessibility. All figures referred to as Supporting Information are available as electronic supplementary material.

Author's contributions. All authors contributed to planning the experiments. O.M.V. and D.A.O. extracted and characterized the samples. O.M.V. carried out statistical analysis. O.M.V and E.D.C drafted the manuscript. All authors critically reviewed the manuscript and provided final approval for publication.

Competing interests. There are no competing interests to declare for the publication of this article.

Funding. This research was made possible through funding from NSERC, Schlumberger and the government of Ontario.

Acknowledgements. Special thanks to Profs R. Pelton, A. Adronov and A. Guarne for the use of equipment and to Drs J. Godoy-Vargas, A. Yakovlev, M. Panga and V. Lafitte for thoughtful discussion and research direction. Victoria Jarvis is acknowledged for performing XRD measurements and fittings. Urooj Gill is acknowledged for imaging cellulose fibres via optical microscopy.

References

1. Nickerson RF, Habrle JA. 1947 Cellulose intercrystalline structure. *Ind. Eng. Chem.* **39**, 1507–1512. (doi:10.1021/ie50455a024)
2. Rånby BG, Banderet A, Sillén LG. 1949 Aqueous colloidal solutions of cellulose micelles. *Acta Chem. Scand.* **3**, 649–650. (doi:10.3891/acta.chem.scand.03-0649)
3. Mukherjee SM, Woods HJ. 1953 X-ray and electron microscope studies of the degradation of cellulose by sulphuric acid. *Biochim. Biophys. Acta* **10**, 499–511. (doi:10.1016/0006-3002(53)90295-9)
4. Reid MS, Villalobos M, Cranston ED. 2017 Benchmarking cellulose nanocrystals: from the laboratory to industrial production. *Langmuir* **33**, 1583–1598. (doi:10.1021/acs.langmuir.6b03765)
5. Habibi Y, Lucia LA, Rojas OJ. 2010 Cellulose nanocrystals: chemistry, self-assembly, and applications. *Chem. Rev.* **110**, 3479–3500. (doi:10.1021/cr900339w)
6. Sacui IA, Nieuwendaal RC, Burnett DJ, Stranick SJ, Jorfi M, Weder C, Foster EJ, Olsson RT, Gilman JW. 2014 Comparison of the properties of cellulose nanocrystals and cellulose

nanofibrils isolated from bacteria, tunicate, and wood processed using acid, enzymatic, mechanical, and oxidative methods. *ACS Appl. Mater. Interfaces* **6**, 6127–6138. (doi:10.1021/am500359f)
7. Camarero Espinosa S, Kuhnt T, Foster EJ, Weder C. 2013 Isolation of thermally stable cellulose nanocrystals by phosphoric acid hydrolysis. *Biomacromolecules* **14**, 1223–1230. (doi:10.1021/bm400219u)
8. Sadeghifar H, Filpponen I, Clarke SP, Brougham DF, Argyropoulos DS. 2011 Production of cellulose nanocrystals using hydrobromic acid and click reactions on their surface. *J. Mater. Sci.* **46**, 7344–7355. (doi:10.1007/s10853-011-5696-0)
9. Yu H-Y, Zhang D-Z, Lu F-F, Yao J. 2016 New approach for single-step extraction of carboxylated cellulose nanocrystals for their use as adsorbents and flocculants. *ACS Sustain. Chem. Eng.* **4**, 2632–2643. (doi:10.1021/acssuschemeng.6b00126)
10. Chen L, Zhu JY, Baez C, Kitin P, Elder T. 2016 Highly thermal-stable and functional cellulose nanocrystals and nanofibrils produced using fully recyclable organic acids. *Green Chem.* **18**, 3835–3843. (doi:10.1039/C6GC00687F)
11. Peng BL, Dhar N, Liu HL, Tam KC. 2011 Chemistry and applications of nanocrystalline cellulose and its derivatives: a nanotechnology perspective. *Can. J. Chem. Eng.* **89**, 1191–1206. (doi:10.1002/cjce.20554)
12. Habibi Y. 2014 Key advances in the chemical modification of nanocelluloses. *Chem. Soc. Rev.* **43**, 1519–1542. (doi:10.1039/C3CS60204D)
13. Dong XM, Revol J-F, Gray DG. 1998 Effect of microcrystallite preparation conditions on the formation of colloid crystals of cellulose. *Cellulose* **5**, 19–32. (doi:10.1023/A:1009260511939)
14. Beck-Candanedo S, Roman M, Gray DG. 2005 Effect of reaction conditions on the properties and behavior of wood cellulose nanocrystal suspensions. *Biomacromolecules* **6**, 1048–1054. (doi:10.1021/bm049300p)
15. Bondeson D, Mathew A, Oksman K. 2006 Optimization of the isolation of nanocrystals from microcrystalline cellulose by acid hydrolysis. *Cellulose* **13**, 171–180. (doi:10.1007/s10570-006-9061-4)
16. Hamad WY, Hu TQ. 2010 Structure–process–yield interrelations in nanocrystalline cellulose extraction. *Can. J. Chem. Eng.* **88**, 392–402. (doi:10.1002/cjce.20298)
17. Kargarzadeh H, Ahmad I, Abdullah I, Dufresne A, Zainudin SY, Sheltami RM. 2012 Effects of hydrolysis conditions on the morphology, crystallinity, and thermal stability of cellulose nanocrystals extracted from kenaf bast fibers. *Cellulose* **19**, 855–866. (doi:10.1007/s10570-012-9684-6)
18. Wang Q, Zhao X, Zhu JY. 2014 Kinetics of strong acid hydrolysis of a bleached kraft pulp for producing cellulose nanocrystals (CNCs). *Ind. Eng. Chem. Res.* **53**, 11 007–11 014. (doi:10.1021/ie501672m)
19. Chen L, Wang Q, Hirth K, Baez C, Agarwal UP, Zhu JY. 2015 Tailoring the yield and characteristics of wood cellulose nanocrystals (CNC) using concentrated acid hydrolysis. *Cellulose* **22**, 1753–1762. (doi:10.1007/s10570-015-0615-1)
20. Dong S, Bortner MJ, Roman M. 2016 Analysis of the sulfuric acid hydrolysis of wood pulp for cellulose nanocrystal production: a central composite design study. *Ind. Crops Prod.* **93**, 76–87. (doi:10.1016/j.indcrop.2016.01.048)
21. Kandola BK, Horrocks AR, Price D, Coleman GV. 1996 Flame-retardant treatments of cellulose and their influence on the mechanism of cellulose pyrolysis. *J. Macromol. Sci. Part C* **36**, 721–794. (doi:10.1080/15321799608014859)
22. Shi Y, Belosinschi D, Brouillette F, Belfkira A, Chabot B. 2014 Phosphorylation of kraft fibers with phosphate esters. *Carbohydr. Polym.* **106**, 121–127. (doi:10.1016/j.carbpol.2014.01.070)
23. Blanchard EJ, Graves EE. 2003 Phosphorylation of cellulose with some phosphonic acid derivatives. *Text. Res. J.* **73**, 22–26. (doi:10.1177/004051750307300104)
24. Božič M, Liu P, Mathew AP, Kokol V. 2014 Enzymatic phosphorylation of cellulose nanofibers to new highly-ions adsorbing, flame-retardant and hydroxyapatite-growth induced natural nanoparticles. *Cellulose* **21**, 2713–2726. (doi:10.1007/s10570-014-0281-8)
25. Ghanadpour M, Carosio F, Larsson PT, Wågberg L. 2015 Phosphorylated cellulose nanofibrils: a renewable nanomaterial for the preparation of intrinsically flame-retardant materials. *Biomacromolecules* **16**, 3399–3410. (doi:10.1021/acs.biomac.5b01117)

26. Hong L, Wang YL, Jia SR, Huang Y, Gao C, Wan YZ. 2006 Hydroxyapatite/bacterial cellulose composites synthesized via a biomimetic route. *Mater. Lett.* **60**, 1710–1713. (doi:10.1016/j.matlet.2005.12.004)
27. Wan YZ, Hong L, Jia SR, Huang Y, Zhu Y, Wang YL, Jiang HJ. 2006 Synthesis and characterization of hydroxyapatite–bacterial cellulose nanocomposites. *Compos. Sci. Technol.* **66**, 1825–1832. (doi:10.1016/j.compscitech.2005.11.027)
28. Wan YZ, Huang Y, Yuan CD, Raman S, Zhu Y, Jiang HJ, He F, Gao C. 2007 Biomimetic synthesis of hydroxyapatite/bacterial cellulose nanocomposites for biomedical applications. *Mater. Sci. Eng. C* **27**, 855–864. (doi:10.1016/j.msec.2006.10.002)
29. Yamaguchi K, Prabakaran M, Ke M, Gang X, Chung IM, Um IC, Gopiraman M, Kim IS. 2016 Highly dispersed nanoscale hydroxyapatite on cellulose nanofibers for bone regeneration. *Mater. Lett.* **168**, 56–61. (doi:10.1016/j.matlet.2016.01.010)
30. Koshizawa T. 1960 Degradation of wood cellulose and cotton linters in phosphoric acid. *Japan Tappi J.* **14**, 455–458, 475. (doi:10.2524/jtappij.14.455)
31. Usuda M, Suzuki O, Nakano J, Migita N. 1967 Acid hydrolysis of cellulose in concentrated phosphoric acid; influences of modified groups of cellulose on the rate of hydrolysis. *J. Soc. Chem. Ind. Japan* **70**, 349–352. (doi:10.1246/nikkashi1898.70.3_349)
32. Li S, Li C, Li C, Yan M, Wu Y, Cao J, He S. 2013 Fabrication of nano-crystalline cellulose with phosphoric acid and its full application in a modified polyurethane foam. *Polym. Degrad. Stab.* **98**, 1940–1944. (doi:10.1016/j.polymdegradstab.2013.06.017)
33. Tang Y, Shen X, Zhang J, Guo D, Kong F, Zhang N. 2015 Extraction of cellulose nano-crystals from old corrugated container fiber using phosphoric acid and enzymatic hydrolysis followed by sonication. *Carbohydr. Polym.* **125**, 360–366. (doi:10.1016/j.carbpol.2015.02.063)
34. Zhang Y-HP, Cui J, Lynd LR, Kuang LR. 2006 A transition from cellulose swelling to cellulose dissolution by *o*-phosphoric acid: evidence from enzymatic hydrolysis and supramolecular structure. *Biomacromolecules* **7**, 644–648. (doi:10.1021/bm050799c)
35. Brinkmann A, Chen M, Couillard M, Jakubek ZJ, Leng T, Johnston LJ. 2016 Correlating cellulose nanocrystal particle size and surface area. *Langmuir* **32**, 6105–6114. (doi:10.1021/acs.langmuir.6b01376)
36. Bhattacharjee S. 2016 DLS and zeta potential—what they are and what they are not? *J. Control. Release* **235**, 337–351. (doi:10.1016/j.jconrel.2016.06.017)
37. Briggs AP. 1922 A colorimetric method for the determination of homogentisic acid in urine. *J. Biol. Chem.* **51**, 453–454.
38. Berenblum I, Chain E. 1938 An improved method for the colorimetric determination of phosphate. *Biochem. J.* **32**, 295–298. (doi:10.1042/bj0320295)
39. Dickman SR, Bray RH. 1940 Colorimetric determination of phosphate. *Ind. Eng. Chem. Anal. Ed.* **12**, 665–668. (doi:10.1021/ac50151a013)
40. Ormaza-González FI, Villalba-Flor AP. 1994 The measurement of nitrite, nitrate and phosphate with test kits and standard procedures: a comparison. *Water Res.* **28**, 2223–2228. (doi:10.1016/0043-1354(94)90035-3)
41. Driemeier C, Calligaris GA. 2011 Theoretical and experimental developments for accurate determination of crystallinity of cellulose I materials. *J. Appl. Crystallogr.* **44**, 184–192. (doi:10.1107/S0021889810043955)
42. Ahvenainen P, Kontro I, Svedström K. 2016 Comparison of sample crystallinity determination methods by X-ray diffraction for challenging cellulose I materials. *Cellulose* **23**, 1073–1086. (doi:10.1007/s10570-016-0881-6)
43. Sasaki M, Kabyemela B, Malaluan R, Hirose S, Takeda N, Adschiri T, Arai K. 1998 Cellulose hydrolysis in subcritical and supercritical water. *J. Supercrit. Fluids* **13**, 261–268. (doi:10.1016/S0896-8446(98)00060-6)
44. Mijares RM, Park GL, Nelson DB, McIver RC. 1986 HPLC analysis of HMF in orange juice. *J. Food Sci.* **51**, 843–844. (doi:10.1111/j.1365-2621.1986.tb13949.x)
45. Porretta S, Sandei L. 1991 Determination of 5-(hydroxymethyl)-2-furfural (HMF) in tomato products: proposal of a rapid HPLC method and its comparison with the colorimetric method. *Food Chem.* **39**, 51–57. (doi:10.1016/0308-8146(91)90084-2)
46. Zappalà M, Fallico B, Arena E, Verzera A. 2005 Methods for the determination of HMF in honey: a comparison. *Food Control* **16**, 273–277. (doi:10.1016/j.foodcont.2004.03.006)

47. Wang N, Ding E, Cheng R. 2007 Thermal degradation behaviors of spherical cellulose nanocrystals with sulfate groups. *Polymer* **48**, 3486–3493. (doi:10.1016/j.polymer.2007.03.062)
48. Daruwalla EH, Shet RT. 1962 Heterogeneous acid hydrolysis of alpha-cellulose from Sudanese cotton. *Text. Res. J.* **32**, 942–954. (doi:10.1177/004051756203201110)
49. Shinoda R, Saito T, Okita Y, Isogai A. 2012 Relationship between length and degree of polymerization of TEMPO-oxidized cellulose nanofibrils. *Biomacromolecules* **13**, 842–849. (doi:10.1021/bm2017542)
50. Fengel D, Wegener G. 1983 *Wood: chemistry, ultrastructure, reactions*. Berlin, Germany: Walter de Gruyter.
51. Jiang F, Esker AR, Roman M. 2010 Acid-catalyzed and solvolytic desulfation of H_2SO_4-hydrolyzed cellulose nanocrystals. *Langmuir* **26**, 17 919–17 925. (doi:10.1021/la1028405)
52. Abitbol T, Kloser E, Gray DG. 2013 Estimation of the surface sulfur content of cellulose nanocrystals prepared by sulfuric acid hydrolysis. *Cellulose* **20**, 785–794. (doi:10.1007/s10570-013-9871-0)
53. Cherhal F, Cousin F, Capron I. 2015 Influence of charge density and ionic strength on the aggregation process of cellulose nanocrystals in aqueous suspension, as revealed by small-angle neutron scattering. *Langmuir* **31**, 5596–5602. (doi:10.1021/acs.langmuir.5b00851)
54. Van Mao RL, Zhao Q, Dima G, Petraccone D. 2011 New process for the acid-catalyzed conversion of cellulosic biomass (AC3B) into alkyl levulinates and other esters using a unique one-pot system of reaction and product extraction. *Catal. Lett.* **141**, 271–276. (doi:10.1007/s10562-010-0493-y)
55. Revol J-F, Bradford H, Giasson J, Marchessault RH, Gray DG. 1992 Helicoidal self-ordering of cellulose microfibrils in aqueous suspension. *Int. J. Biol. Macromol.* **14**, 170–172. (doi:10.1016/S0141-8130(05)80008-X)
56. Cherif M, Mgaidi A, Ammar N, Vallée G, Fürst W. 2000 A new investigation of aqueous orthophosphoric acid speciation using Raman spectroscopy. *J. Solution Chem.* **29**, 255–269. (doi:10.1023/A:1005150400746)
57. Mesmer RE, Baes CF. 1974 Phosphoric acid dissociation equilibria in aqueous solutions to 300°C. *J. Solution Chem.* **3**, 307–322. (doi:10.1007/BF00648228)
58. Elmore KL, Hatfield JD, Dunn RL, Jones AD. 1965 Dissociation of phosphoric acid solutions at 25°. *J. Phys. Chem.* **69**, 3520–3525. (doi:10.1021/j100894a045)